Journal of Chromatography, 459 (1988) 119–138
Elsevier Science Publishers B.V., Amsterdam — Printed in The Netherlands

CHROMSYMP. 1467

EXPERIMENTAL AND THEORETICAL MODEL OF REFRACTIVE INDEX ARTIFACTS IN ABSORBANCE DETECTION

CHRISTINE E. EVANS, JOHN G. SHABUSHNIG* and VICTORIA L. McGUFFIN*
Department of Chemistry, Michigan State University, East Lansing, MI 48824 (U.S.A.)

SUMMARY

An anomalous signal is often observed upon sample injection in both liquid chromatography and flow-injection analysis using high-sensitivity absorbance detectors. This characteristic detector response, unrelated to sample absorbance, appears to arise from the change in refractive index within the flowcell. The factors affecting the refractive index gradient have been incorporated in a ray-tracing model, where the flowcell is regarded as a dynamic lens. The response predicted by this model correlates well with experimental measurement of the general shape, magnitude, and direction of the refractive index artifact. The proposed model should have wide ranging implications for both flowcell design and chromatographic interpretation of these anomalous signals.

INTRODUCTION

Detection systems based on absorption of electromagnetic radiation in the ultraviolet or visible region are among the most widely used in liquid chromatography (LC). Ideally, absorbance detectors respond only to substances which absorb the source radiation at a specific wavelength. However, an anomalous and non-specific response is commonly observed in high-sensitivity applications due to refractive index effects. A change in refractive index within the flowcell causes reflection and refraction of source radiation, resulting in a change in light intensity at the photodiode detector. This anomalous response is observed under a variety of experimental conditions, including sample injection (Fig. 1), stepwise or linear gradient elution, and other rapid changes in solvent composition. These refractive index artifacts can interfere with solute detection, leading to confusion or misinterpretation of chromatographic data.

Although commonly observed in LC[1] as well as flow-injection applications[2], the exact nature of the refractive index artifact is not clearly understood. Many factors are thought to affect the shape, magnitude, and direction of this response. The influence of flowcell geometry has been examined for cylindrical and square capillaries[3–7], sheath flowcells[6,8], and U- or Z-pattern flowcells[2,9–11]. Design of the external optical system also influences the response, since source radiation may be convergent, divergent, or

* Present address: The Upjohn Company, Kalamazoo, MI 49001, U.S.A.

0021-9673/88/$03.50

Fig. 1. Chromatogram illustrating refractive index artifact occurring in absorbance detection upon injection of standard test mixture dissolved in methanol into a methanol–water (75:25, v/v) mobile phase. Characteristic derivative-shaped response from absorbance anomaly is seen at a retention time of 10 min.

collimated as it enters the flowcell[10]. Finally, the absolute refractive index and refractive index gradient within the flowcell appear to have a substantial effect[10,11].

Although theoretical evaluations of the refractive index dependence of flowcells have been presented[2–11], attempts to correlate theoretical predictions and experimental results have been notably scarce in the literature. In this work, a three-fold approach is used to elucidate this detection anomaly. First, an absorbance detector with Z-pattern flowcell is utilized to measure the experimental shape, magnitude, and direction of the refractive index response occurring upon injection. Second, the change in light throughput in the flowcell is monitored by direct visual and photographic inspection to determine the origin of the detector response. Finally, optical ray-tracing techniques are employed to simulate the image diameter and intensity resulting from the refractive index gradient in the flowcell. Although the development presented here is limited to injection profiles in the Z-pattern flowcell, this approach should be applicable to any gradient or flowcell of interest.

THEORY

At the interface between two homogeneous media of differing refractive index (n), an incident light ray is deflected at an angle (θ) according to Snell's law:

$$n_1 \sin\theta_1 = n_2 \sin\theta_2 \quad (1)$$

When a flowcell is an integral part of an optical system, the refractive index properties within the cell determine the angular deflection of incident light. This deflection determines the size of the detected image and, if the flowcell is the limiting aperture in the system, the overall intensity of that image. Accordingly, in a flowcell containing a static or flowing solution of constant composition, the resulting transmittance depends on the absolute refractive index of the medium. However, when a zone of different composition is injected into the flowing stream, concentration gradients are formed by laminar flow, diffusion, and mixing phenomena. Because refractive index is a function of concentration, a corresponding refractive index profile is generated with components both radial and axial to the direction of flow. As the zone traverses the flowcell, the angular deflection of the incident light rays varies continuously in time and space, causing the flowcell to act as a dynamic gradient-index lens. The resultant response in such a dynamic system depends on the gradient of refractive index present in the flowcell, not on the absolute refractive index. Thus, determination of the final image size and intensity requires knowledge of both radial and axial contributions to the refractive index gradient.

The mathematical form of the radial gradient (dn/dr), which is perpendicular to the axis of flow, can be expressed as the product:

$$\frac{dn}{dr} = \frac{dn}{dC} \cdot \frac{dC}{dr} \tag{2}$$

where dn/dC represents the change in refractive index with concentration, and dC/dr is the change in concentration across the flowcell radius. Similarly, the axial gradient (dn/dz) can be determined from the change in concentration parallel to the axis of flow (dC/dz):

$$\frac{dn}{dz} = \frac{dn}{dC} \cdot \frac{dC}{dz} \tag{3}$$

Detailed knowledge of the form of the individual differential equations, as described below, is necessary to determine the radial and axial refractive index gradients.

Evaluation of dn/dC

According to simple solution theory, the refractive index of binary mixtures is a linear function of concentration[12], so that dn/dC is a constant. However, such ideal behavior is rarely observed for the polar, highly interacting solvents of interest in liquid chromatography (Fig. 2). For non-ideal solvent mixtures, dn/dC must be calculated from the tangential slope of the graph of refractive index *versus* concentration. This is achieved by reducing the experimental data to a polynomial equation and, subsequently, calculating the derivative (dn/dC) as a function of concentration.

Evaluation of dC/dr

For a flowcell of cylindrical geometry, the radial concentration gradient (dC/dr) can be determined from the equation derived by Taylor[13]:

$$C = C_0 + \frac{R^2 u}{4D_m}\left(\frac{r^2}{R^2} - \frac{r^4}{2R^4}\right)\frac{dC_0}{dz} \tag{4}$$

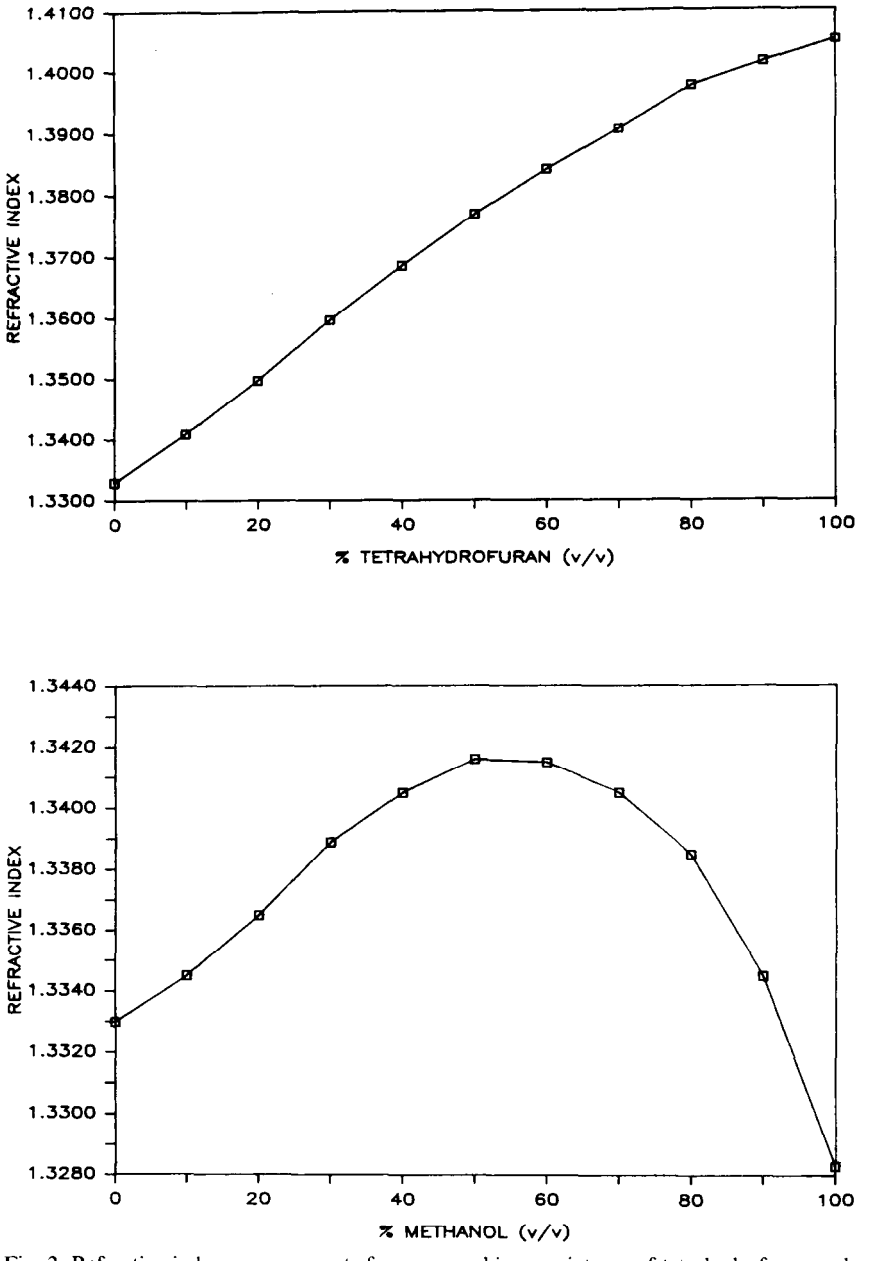

Fig. 2. Refractive index measurements for aqueous binary mixtures of tetrahydrofuran and methanol.

where the concentration (C) at a given radial distance (r) is evaluated as a function of the concentration (C_0) and axial concentration gradient (dC_0/dz) at the tube center, the tube radius (R), linear velocity (u), and diffusion coefficient (D_m). If the residence time in the flowcell is short, the concentration profile may be modelled as a parabola by

neglecting the second term of the parenthetical expression in eqn. 4. The derivative (dC/dr) is then evaluated as a function of the radial position.

Evaluation of dC/dz

The axial concentration function can take various forms for the injection and gradient elution profiles encountered in liquid chromatography. For an ideal injection, the concentration profile upon leaving the chromatographic column can be modelled as a Gaussian function:

$$C = \frac{M}{(2\pi\sigma_L^2)^{1/2}(\pi R^2)} \exp\left(\frac{-z^2}{2\sigma_L^2}\right) \quad (5)$$

where M is the injected sample mass, and z is the axial distance from the center of a zone with length variance σ_L^2. The length variance of the zone can be estimated from the Golay equation[14] for an open-tubular column, or from the Van Deemter[15] or Knox[16] equations for a packed column. The concentration gradient (dC/dz) is then calculated as a function of the axial position.

For the ideal conditions described herein, the radial refractive index gradient (dn/dr) can be determined by eqn. 2 from the derivative of the radial concentration profile (dC/dr) given in eqn. 4 and the dependence of refractive index on concentration (dn/dC). Similarly, the axial refractive index gradient (dn/dz) can be calculated by eqn. 3 from the axial concentration gradient (dC/dz) for injection given by eqn. 5 and the (dn/dC) relationship. Consequently, the absolute refractive index at specific coordinates (r,z) in the flowcell can be determined by integration, and the angular deflection subsequently calculated by using Snell's law (eqn. 1). Unfortunately, these differential equations are not readily amenable to analytical solution. In this paper, we have approached this problem by incorporating the calculated gradients into a simulation model based on optical ray tracing, where the flowcell is regarded as a dynamic lens. Although the assumed form of these gradients is greatly simplified, this model allows the direct comparison of theoretical predictions with experimental measurements of refractive index artifacts present in absorbance detection.

EXPERIMENTAL

Reagents

All organic solvents were high-purity, distilled-in-glass grade (Burdick and Jackson, Muskegon, MI, U.S.A.). Water was deionized and doubly distilled in glass (Model MP-3A, Corning Glass Works, Corning, NY, U.S.A.). Binary aqueous solutions of the organic solvents, ranging from 0 to 100% (v/v) were prepared by thoroughly mixing known volumes of each component.

Refractive index measurements

Measurements of refractive index were performed in triplicate utilizing an Abbe refractometer (Model Abbe-3L, Bausch and Lomb, Rochester, NY, U.S.A.), maintained at 25.0°C. Reproducibility was better than ± 0.0001 relative standard deviation (R.S.D.) for replicate measurements of a single sample as well as for replicate samples. Results of the refractive index measurements for binary mixtures of tetrahydrofuran–water and methanol–water are summarized in Fig. 2.

Chromatographic detection

A schematic diagram of the experimental system is shown in Fig. 3. A syringe pump (Model μLC-500, Isco, Lincoln, NE, U.S.A.) was utilized for solvent delivery at a constant flow-rate of 50 μl/min. Samples were introduced with a 1-μl injection valve (Model C14W1, Valco Instruments, Houston, TX, U.S.A.), which was connected directly to the detector by using an open tube of 46 cm × 0.025 cm I.D. A commercially available absorbance detector (Model Uvidec 100-V, Jasco, Tokyo, Japan), with a 1-μl Z-pattern flowcell, was employed at a monochromator wavelength of 589 nm with a 500-nm high-pass cutoff filter. This wavelength was chosen to allow the anomalous response due to refractive index to be distinguished from true sample absorbance. The apparent absorbance signal, resulting only from refractive index artifacts, was displayed on a chart recorder (Model 585, Linear Instruments, Reno, NV, U.S.A.) and was converted to transmittance by manual calculation.

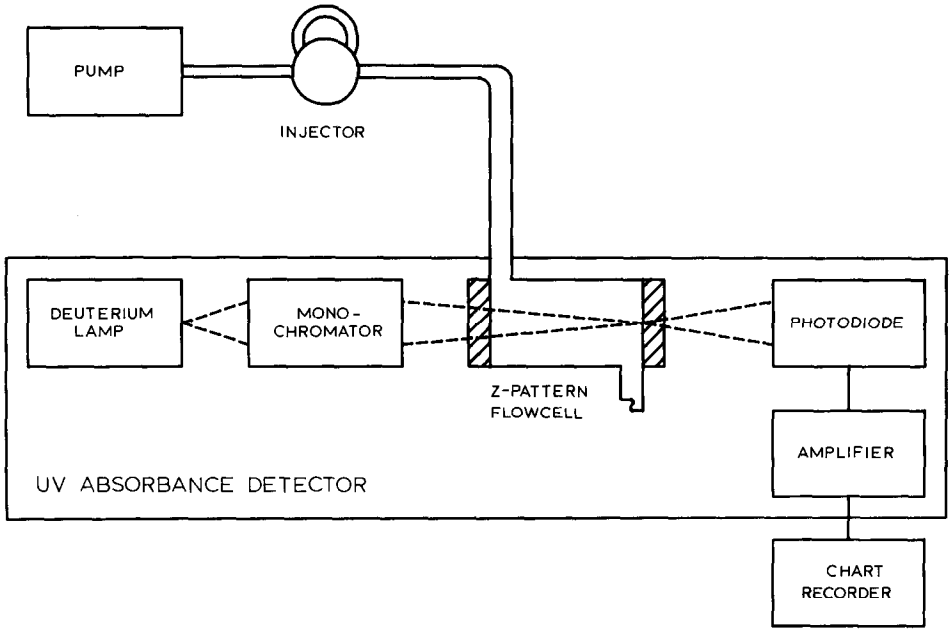

Fig. 3. Schematic diagram of liquid chromatographic absorbance detector. A 500-nm high-pass cutoff filter was placed between the source and monochromator, and measurements performed at 589 nm to isolate the refractive index artifact from response due to absorption of source radiation.

Visual detection

The Z-pattern flowcell was removed from the commercial detector, allowing direct probing of the cell with a helium–neon laser (Model 155, Spectra-Physics, Mountain View, CA, U.S.A.). The laser radiation was focussed on the cell utilizing a quartz lens (1.0 in. focal length, 1.0 in. diameter). The transmitted light was displayed on a viewing screen, placed 85 cm from the flowcell, for direct visual and photographic inspection.

Simulation

The simulation of refractive index artifacts was performed on an IBM-XT microcomputer (International Business Machines, Boca Raton, FL, U.S.A.) with a commercially available software package (Beam3, Stellar Software, Berkeley, CA, U.S.A.). This software allows the placement of optical sources, refracting and reflecting optical elements, apertures, and viewing screens at arbitrary positions. The resultant optical system is then analyzed using a three-dimensional ray-tracing algorithm.

In this simulation, a point source at 589 nm wavelength was located 0.5 mm from the front surface of a Z-pattern flowcell. The flowcell, shown in Fig. 4, was modelled as a pair of quartz windows ($n_D = 1.4570$) of 1.0 mm thickness and 0.5 mm aperture diameter. These parallel windows were separated by a distance of 5.0 mm, within which a flowing solution was contained. Finally, a screen was positioned 25 mm from the rear window of the flowcell to simulate the photodiode.

The flowing solution was modelled as a dynamic lens with continuously varying refractive index in both radial and axial directions. The radial contribution to the

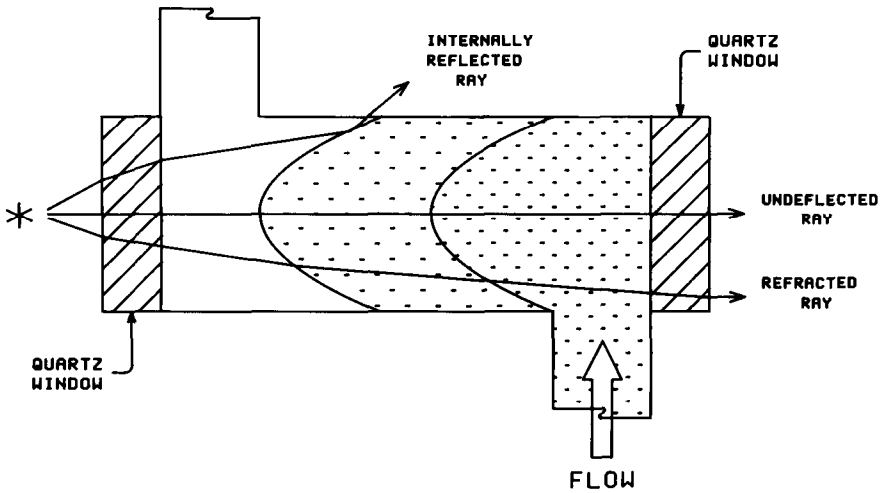

Fig. 4. Illustration of a Z-pattern flowcell with both radial and axial refractive index gradients.

refractive index gradient, which is parabolic in form, was calculated using eqn. 4 neglecting the $r^4/2R^4$ term. This expression defines the shape and curvature of the surfaces of constant concentration $[(C - C_0)/(dC_0/dz)]$, and hence, of constant refractive index, if dC_0/dz is considered constant in the flowcell at any point in time. The curvature of the parabolic profile, which characterizes the radial refractive index gradient, is given in eqn. 4 by the constant $(R^2u/4D_m)$. In this simulation, the flowcell radius ($R = 0.025$ cm) as well as mobile-phase velocity in the flowcell ($u = 0.4$ cm/s) were taken from experimentally measured values. Diffusion coefficients (D_m) were estimated utilizing the Wilke–Chang equation[17] to be $1.08 \cdot 10^{-5}$ cm^2/s for tetrahydrofuran in water and $1.64 \cdot 10^{-5}$ cm^2/s for methanol in water at 25°C.

The axial refractive index gradient was determined from the corresponding axial concentration gradient in eqn. 5, which is Gaussian in form. In order to accomplish this determination, the zone variance (σ_L^2) was first estimated for the open tube connecting the injector and detector using the familiar Taylor–Aris equation[13,18]:

$$\sigma_L^2 = \frac{R_t^2 \; u \; L_t}{24 \; D_m} \tag{6}$$

In this calculation, the tube radius ($R_t = 0.0125$ cm), length ($L_t = 46$ cm), and mobile phase velocity ($u = 1.7$ cm/s) were taken from experimental measurements. The length variance determined for the tetrahydrofuran–water solvent system was 50.8 cm^2 in the connecting tube, which corresponds to 3.17 cm^2 in the cell, while that for the methanol–water system was 31.0 cm^2 in the tube and 1.93 cm^2 in the cell. Subsequently, concentration values were calculated across the Gaussian profile using eqn. 5, in which the sample mass (M) was determined for a 1-μl injection volume, and all other experimental parameters were as previously defined. The limits of the Gaussian profile were assumed to be $6\sigma_L$, where the concentration is 1% of the maximum value at the zone center. Finally, the corresponding refractive indices were determined by interpolation from the concentration values (Fig. 2) as a function of the axial distance along the Gaussian profile.

After calculation of the radial and axial refractive index gradients was completed, the simulation was performed by sequentially incrementing the calculated axial refractive index profile through the flowcell in a stepwise manner. A minimum of 40 points was evenly distributed across the Gaussian profile at a constant axial interval of 2 mm, which corresponds to approximately 0.15 σ_L. At each point, both the final image size and intensity were assessed with the Beam3 ray-tracing software. The diameter of the image was determined by evaluating the position of a single peripheral ray on the detection screen. Image intensity values were calculated by allowing 1000 rays (I_0) of randomly distributed angles to be incident on the entrance of the flowcell. The number of rays transmitted through the cell (I) was subsequently determined and

TABLE I

COMPARISON OF NORMALIZED EXPERIMENTAL AND SIMULATED IMAGE INTENSITY AND SIZE FOR INJECTION RESPONSE OF TETRAHYDROFURAN–WATER SYSTEM

		Tetrahydrofuran injected into water		*Water injected into tetrahydrofuran*	
		First deflection	*Second deflection*	*First deflection*	*Second deflection*
Image intensity	Experimental	1.14	0.85	0.91	1.04
	Simulated	1.36	0.76	0.83	1.12
Image size	Experimental	0.56	1.53	1.10	0.91
	Simulated	0.81	1.20	1.09	0.91

TABLE II

COMPARISON OF NORMALIZED EXPERIMENTAL AND SIMULATED IMAGE INTENSITY AND SIZE FOR INJECTION RESPONSE OF METHANOL–WATER SYSTEM

		Methanol injected into water		*Water injected into methanol*	
		First deflection	*Second deflection*	*First deflection*	*Second deflection*
Image intensity	Experimental	1.05	0.97	1.10	0.89
	Simulated	1.06	0.96	1.24	0.82
Image size	Experimental	0.82	1.14	0.90	1.30
	Simulated	0.96	1.04	0.84	1.16

the image intensity ratio (I/I_0) calculated. This simulated intensity ratio was then normalized to that for the mobile-phase solvent. Because transmittance (T) is defined as the ratio of the transmitted power (P) to the incident power (P_0), intensity ratios predicted from the simulation (I/I_0) can be directly compared with experimental measurements of transmittance (P/P_0), which have been likewise normalized (Table I and II).

RESULTS AND DISCUSSION

In order to examine refractive index artifacts in absorbance detection, systematic experimental and theoretical studies of the response occurring upon injection were undertaken. The two solvent systems chosen for these studies, tetrahydrofuran–water and methanol–water, are representative of the wide variety of refractive index conditions encountered in reversed-phase LC. Not only is the range of absolute refractive indices among these solvents substantial (1.3328 for methanol, 1.3330 for water, and 1.4051 for tetrahydrofuran at 25°C), but the dependence of refractive index on concentration is notably different for the two solvent systems (Fig. 2). Aqueous mixtures of tetrahydrofuran show nearly ideal, linear refractive index response as a function of concentration, while aqueous methanol mixtures exhibit distinctly non-ideal behavior. Thus, these two solvent systems allow the characterization of this anomaly under the variety of refractive index conditions encountered in reversed-phase separations.

Experimental results

A commercially available absorbance detector equipped with a Z-pattern flowcell was utilized to evaluate the anomalous refractive index signal occurring upon injection of pure solvents. The detector response, displayed as the transmittance relative to that of the mobile phase, is shown in Fig. 5 for the tetrahydrofuran–water system. Upon injection of tetrahydrofuran into water (Fig. 5A), a derivative-shaped signal was observed with an absolute magnitude of approximately 0.08 absorbance units peak to peak. The direction of this signal shows first an increase (+) then

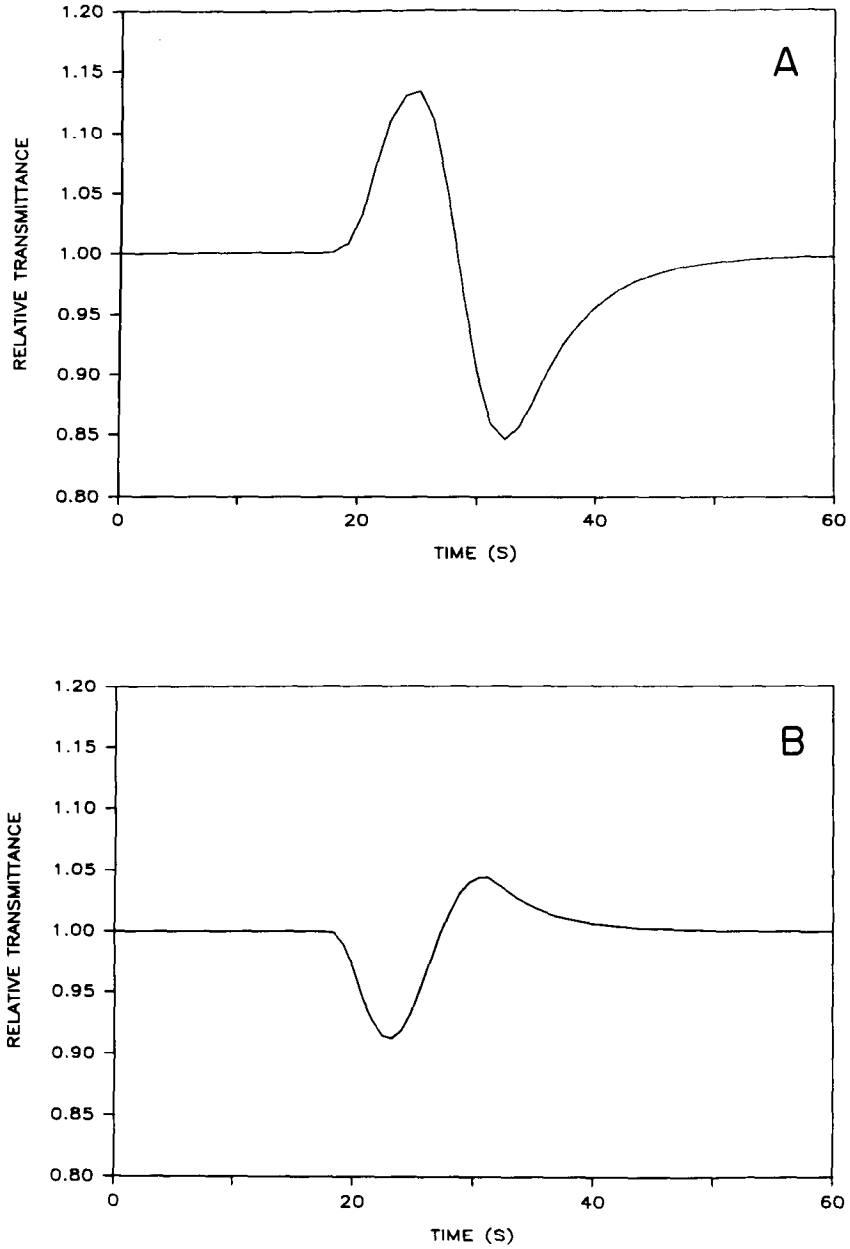

Fig. 5. Experimentally measured relative transmittance response occurring upon injection of (A) tetrahydrofuran into water and (B) water into tetrahydrofuran. Injection volume, 1 μl; flow-rate, 50 μl/min; detector volume, 1 μl; monochromator wavelength, 589 nm.

a decrease (−) in the relative transmittance. In contrast, when water was injected into tetrahydrofuran (Fig. 5B), the magnitude of the signal was reduced and the direction of signal deflection was reversed (−/+). The first and second deflection, measured at the

extremes of these derivative-shaped signals, are summarized as the normalized intensity in Table I.

Further investigations of this phenomenon were accomplished for the methanol–water system and are summarized in Fig. 6 and Table II. The refractive index

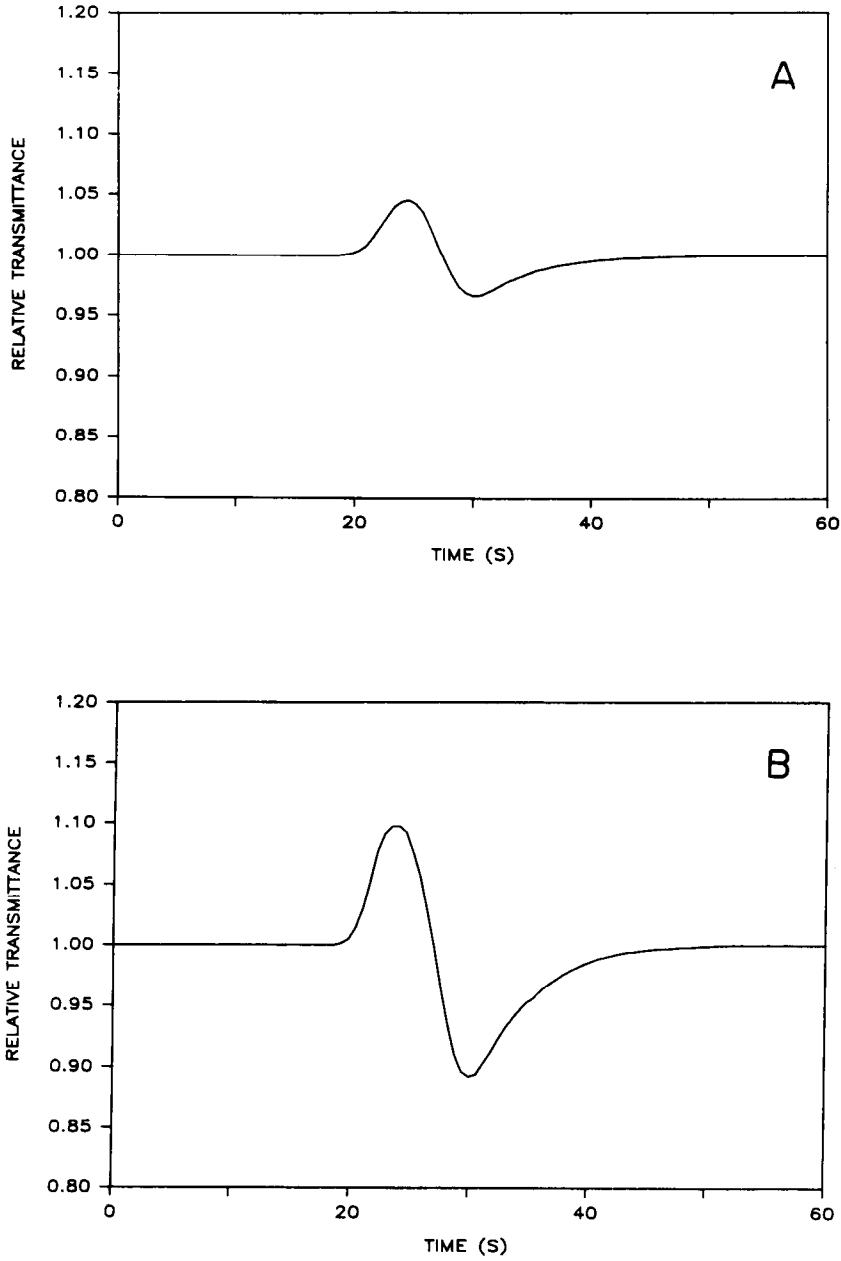

Fig. 6. Experimentally measured relative transmittance response occurring upon injection of (A) methanol into water and (B) water into methanol. Conditions same as for Fig. 5.

artifact observed experimentally was comparable to that of the tetrahydrofuran–water system in both shape and magnitude. In contrast to the tetrahydrofuran–water system, the signals observed for methanol injected into water (Fig. 6A) and water injected into methanol (Fig. 6B) were identical in direction (+/−). This result would not be expected if the response were determined solely by the absolute refractive index of the individual components. Moreover, the characteristic, derivative-shape response is not predictable for either system based on considerations of absolute refractive index alone.

To characterize the source of this derivative-shaped response in greater detail, the Z-pattern flowcell was removed from the absorbance detector and used for direct observation of this phenomenon. Visual detection was accomplished by focussing a helium–neon laser onto the Z-pattern flowcell and viewing the transmitted image on a screen as the zone eluted. Direct photographic monitoring of the injection of tetrahydrofuran into water is shown in a discontinuous time sequence in Fig. 7. The image of the transmitted radiation showed a substantial change in both size and intensity as the tetrahydrofuran zone passed through the flowcell. An initial decrease followed by an increase in image diameter was apparent during elution of the zone. Concurrently, the local light intensity was observed to increase then decrease, consistent with the detector response shown in Fig. 5A. Thus, the anomalous response may result from a change in intensity due to variations in image size or in overall throughput. Since no movement in the position of the resultant spot was visible, these two factors appear to be the primary contributions to detector response.

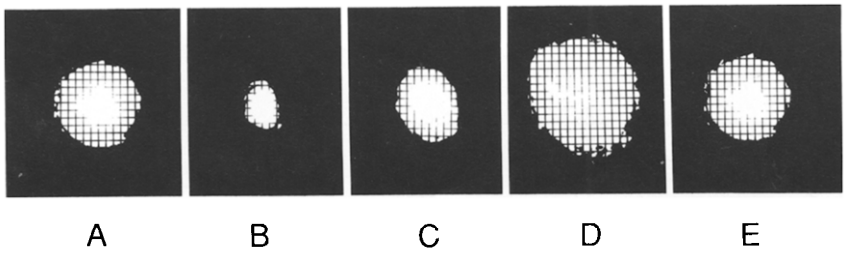

Fig. 7. Time sequence of photographs showing the change in light transmitted through the Z-pattern flowcell upon injection of tetrahydrofuran into a water mobile phase (Fig. 5A), (A) water mobile phase, 17 s; (B) first deflection, 25 s; (C) transition, 29 s; (D) second deflection, 33 s; (E) water mobile phase, 50 s.

Simulation results

Further elucidation of this anomaly was accomplished by computer simulation of the injection process in the Z-pattern flowcell. Dynamic refractive index gradients induced by the concentration profile formed upon injection were simulated with an optical ray-tracing model. This model incorporated refractive index gradients within the cell in both radial and axial directions relative to the axis of flow. In all simulations, the radial refractive index gradient was assumed to be of the parabolic form described by eqn. 4, neglecting the $r^4/2R^4$ term. The axial component of the gradient was determined based on the ideal Gaussian profile given in eqn. 5.

Simulation results are shown for the injection of tetrahydrofuran into water (Fig. 8) and water into tetrahydrofuran (Fig. 9) *versus* normalized axial position (z/σ_L).

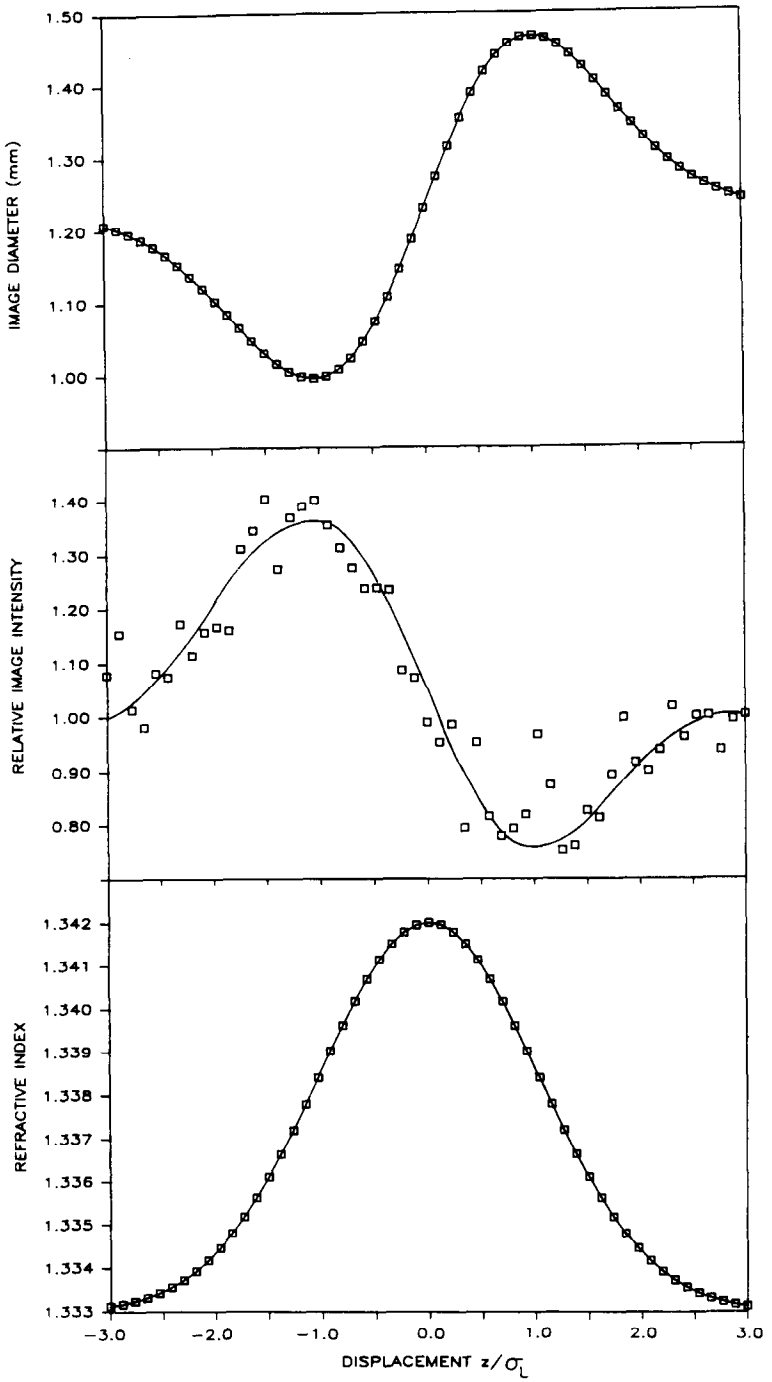

Fig. 8. Simulation results for tetrahydrofuran injected into water. Image diameter and overall relative intensity predicted for axial gradient shown at bottom of figure. Input parameters same as for Fig. 5.

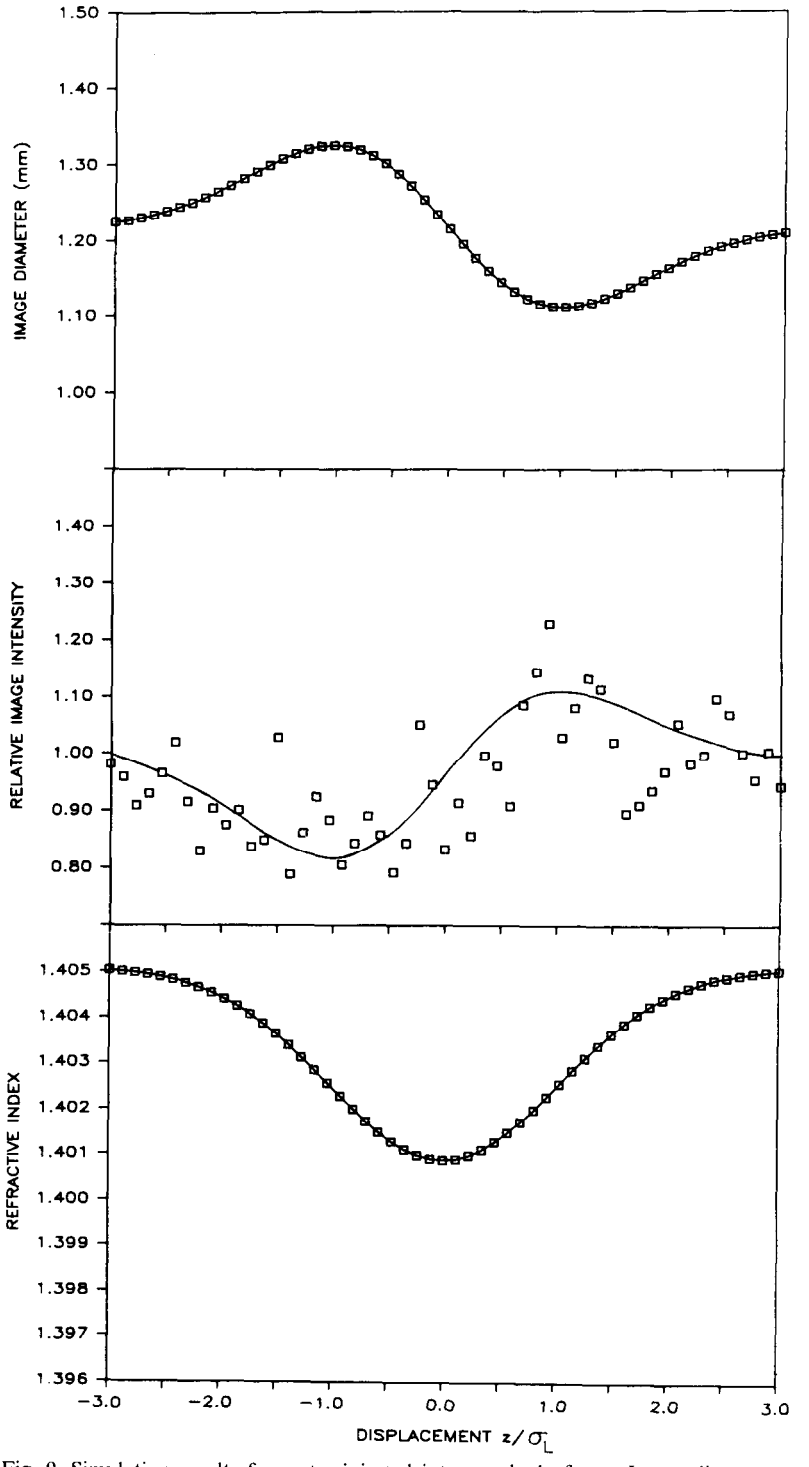

Fig. 9. Simulation results for water injected into tetrahydrofuran. Image diameter and overall relative intensity predicted for axial gradient shown at bottom of figure. Input parameters same as for Fig. 5.

The calculated axial function of refractive index, utilized as input to the simulation, is included along the bottom of each figure for clarity. Predictions of image size (figure top) and overall intensity (figure center) based on this simulation model show the characteristic derivative shape of the refractive index artifact. Relative image size predicted by the model shows good correlation with that determined by visual inspection. These results are summarized in Table I, where the experimental and theoretical relative image sizes are compared at the first and second deflection of the derivative-shaped response. In addition, excellent agreement of predicted and experimental image intensity is apparent by qualitative comparison of Figs. 8 and 9 with Fig. 5, and by quantitative comparison in Table I. Fluctuation in the predicted intensity values (R.S.D. = 6%) is due to variability in the random-number generator utilized for the simulation. Despite this imprecision, these results clearly indicate that changes in both image size and intensity are responsible for the observed refractive index artifacts. The comparison of image size and intensity in Table I provides quantitative confirmation of the accuracy of the simulation model.

As the simulation results for the tetrahydrofuran–water system indicate, the predicted detector response is a direct outcome of the changing focal properties of the "solvent lens" within the cell. At any time during the simulation, only a fraction (7%) of the total axial gradient is contained within the flowcell. Therefore, the steepness of the axial gradient within the flowcell is continuously changing as different portions of the zone traverse the cell. This varying axial gradient, together with a constant radial gradient, continuously alters the angle of light rays traversing the cell. If both components of the gradient are positive, the result based on Snell's law (eqn. 1) is a decrease in image size. When the axial gradient is reversed, as occurs after the midpoint of the Gaussian function, the size of the resultant image becomes larger. This process defines the derivative-shaped response, showing first a decrease followed by an increase in size when the injection profile shows a maximum in refractive index. Under conditions of constant radial gradient (constant flow-rate), the magnitude of this change in size is directly dependent on the magnitude of the axial gradient (dn/dz). This supposition, based on optical considerations, is confirmed in both the simulation and experimental results for the tetrahydrofuran–water system. Although this system has a nearly linear dependence of refractive index on concentration, the magnitude of dn/dC and, hence, dn/dz is greater for injections of tetrahydrofuran into water than for water into tetrahydrofuran (Fig. 2), and the resulting change in image size is proportionally larger. Intensity changes are also directly related to the variations in the angle of the light rays during elution. For the light conditions simulated here, two factors contribute to the change in throughput of the cell. First, the acceptance angle of the cell is directly proportional to the axial refractive index gradient. Because this model utilizes a point source of radiation, as the gradient increases, the amount of light allowed into the cell also increases. Second, the exit of the flowcell can act as the aperture stop, limiting the angle of light rays leaving the flowcell. For an increase in the axial gradient, both these factors lead to an increased light throughput. Thus, the changes in the axial refractive index gradient within the cell alter the angle of light rays, resulting in variations in both the size and intensity of the detected image. Although the dynamic nature of the axial gradient causes these changes in the resultant image, both axial and radial gradients are necessary for this "solvent lens" effect.

To test the versatility of this model, further simulations employed the non-ideal

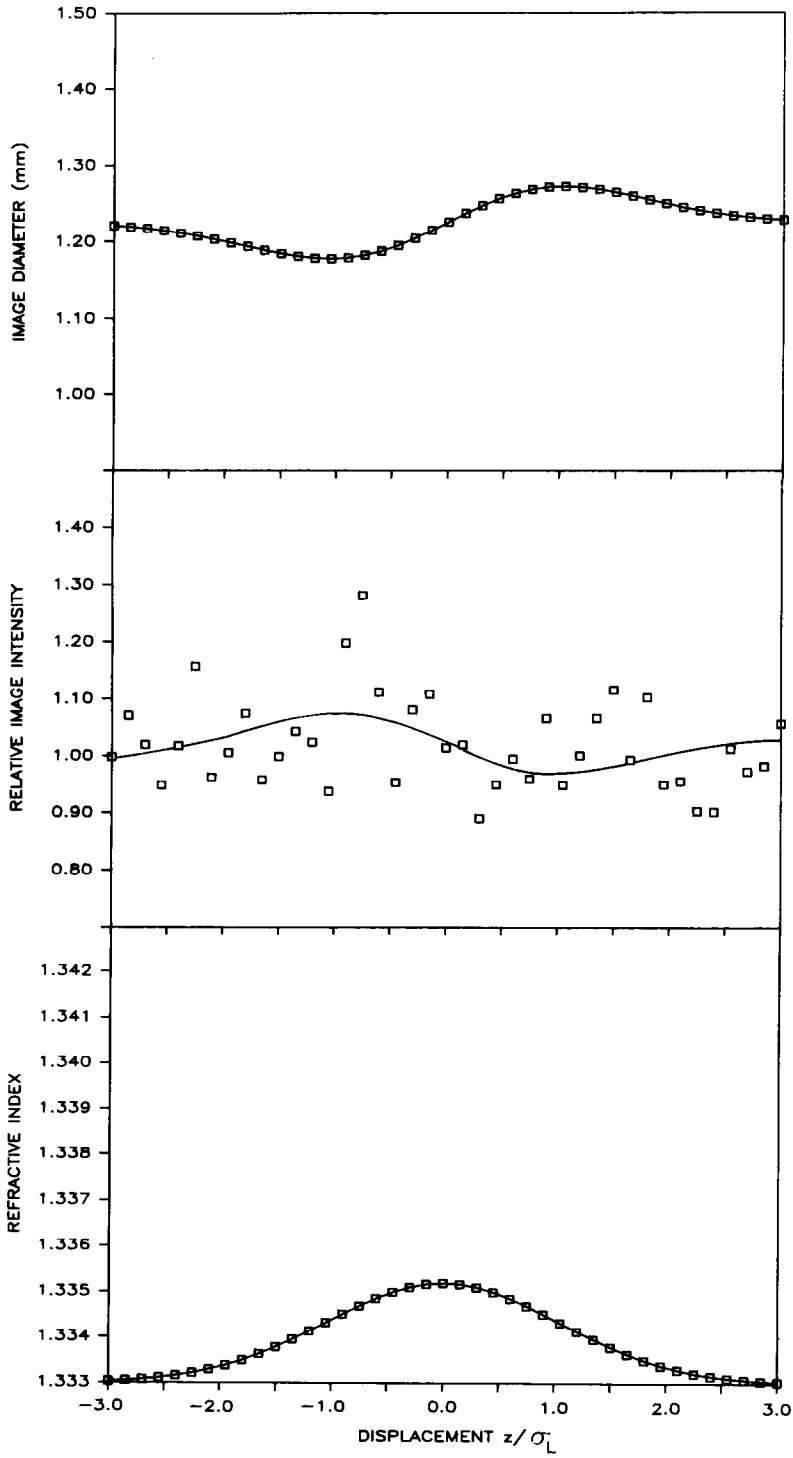

Fig. 10. Simulation results for methanol injected into water. Image diameter and overall relative intensity predicted for axial gradient shown at bottom of figure. Input parameters same as for Fig. 6.

methanol–water solvent system. In contrast to tetrahydrofuran–water, methanol–water exhibits a maximum in refractive index with concentration which is substantially greater than that of either pure solvent (Fig. 2). Yet, the predicted response illustrated in Figs. 10 and 11 shows excellent agreement in general shape and magnitude with the experimental response in Fig. 6. The quantitative comparison of image size and intensity for experimental measurement and theoretical prediction is given in Table II. The most interesting feature of the methanol–water system is that the direction of response (+/−), whether predicted (Figs. 10 and 11) or experimentally observed (Fig. 6), is identical for injection of methanol into water and *vice versa*. This similarity of response direction is a result of the maximum in refractive index *versus* concentration for the methanol–water solvent system. For this system, dn/dC is always positive when the zone profile at the detector has a concentration maximum less than 50% (v/v), even though methanol has a lower absolute refractive index than water. Dispersion of the plug injection for the methanol–water system results in a calculated concentration maximum of 14.6%. Because dC/dz is identical regardless of injection order (methanol–water or water–methanol), dn/dC determines both the sign and magnitude of the axial refractive index gradient (dn/dz). Consequently, dn/dz will always be of the same sign and the refractive index artifact will always be in the same direction. Thus, accurate prediction of even non-ideal solvent systems is possible with this gradient index model.

Limitations of the simulation model

As with any model, some simplifying assumptions are necessary to simulate experimental conditions. In this particular model, most assumptions arise from the flow conditions needed to describe the refractive index gradients induced upon injection of a pure solvent into a flowing stream. Whenever possible, all flow parameters have been chosen to be consistent with those experimentally examined. Concentration gradients are assumed to form from axial dispersion of an instantaneous injection described by the Taylor expression (eqns. 5 and 6). In practice, however, no injection is an ideal delta function and the resultant concentration profile may deviate from the predicted Gaussian shape. Moreover, any exponential mixing occurring in the region between the connecting tube and the flowcell will result in a modified Gaussian profile. A modified profile may indeed be expected due to the change in diameter between the tubing and the flowcell, as well as the right-angle entrance and exit of the Z-pattern flowcell. This abrupt change in flow path may influence not only the axial gradient, but the radial component as well. The Z-pattern design can give rise to an apparent bimodal flow path through the cell which results in complex radial gradients within the detector volume[19]. These gradients are not well understood or well characterized, therefore simulation of flow within the cell is limited at the present time to the parabolic profile described for a straight, round-bore tube.

External optical conditions also play a role in determining the intensity and size of the resultant image. For the simulation presented here, light incident on the flowcell was assumed to be divergent, effectively overfilling the entrance aperture. This is similar to many absorbance detector designs, where the exit of the monochromator acts as a point source of radiation for the flowcell. These light conditions, while true of the present detection system, are not representative of all systems. The model, however, can be adapted to the external optical configuration of any detector design.

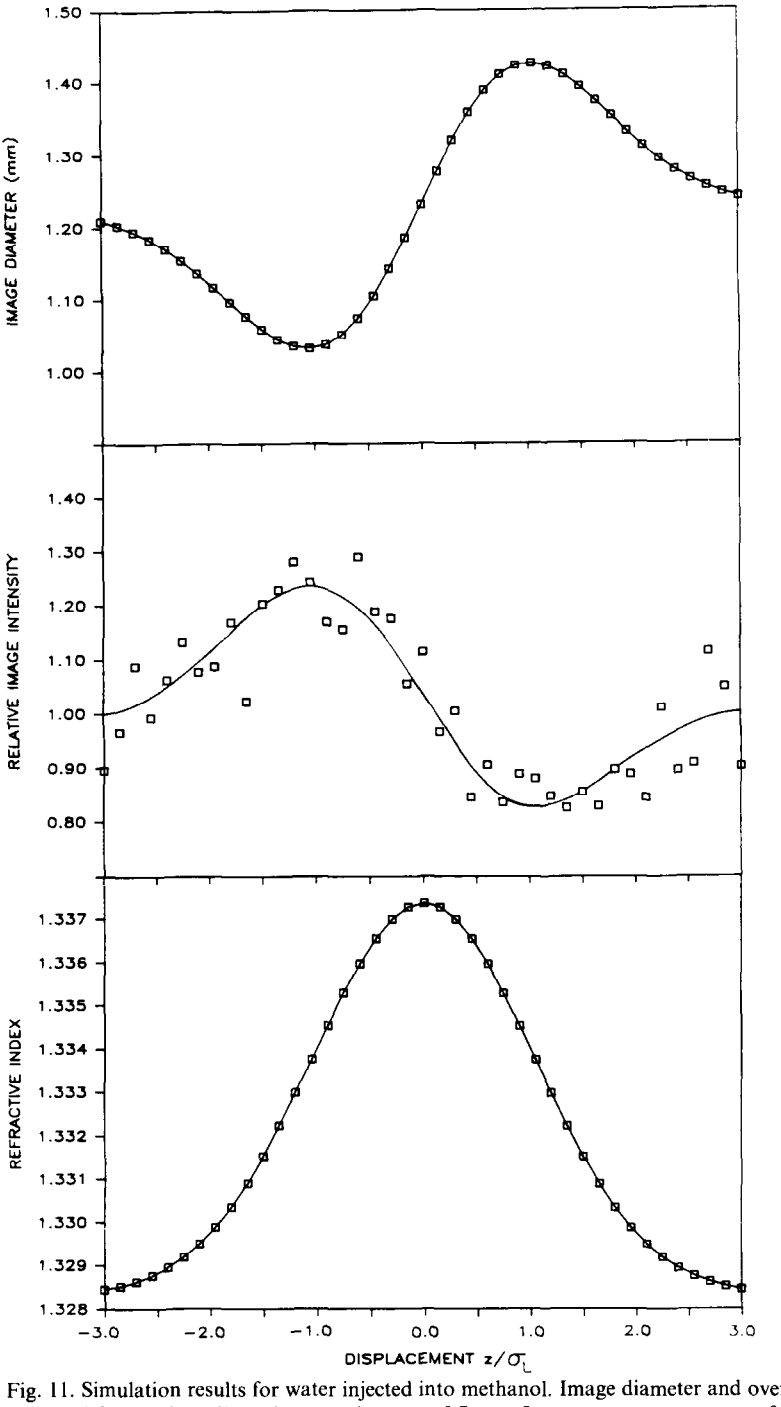

Fig. 11. Simulation results for water injected into methanol. Image diameter and overall relative intensity predicted for axial gradient shown at bottom of figure. Input parameters same as for Fig. 6.

Although the above assumptions have been necessary to describe flow and optical conditions in the detection system, a few additional assumptions have been necessitated by the software package utilized in the simulation. The Beam3 software requires that light rays strike all optical elements in the system in order to be detected. This restriction limits the simulation by not allowing light incident on the flowcell walls to continue through the simulated optical system. This is not true in many real flowcell designs, which contain polished interior walls allowing reflection of light. This assumption should result in attenuation of the simulated response, but the shape and direction of the signal would remain unchanged. In addition, the Beam3 software requires that the axial gradient be sequentially incremented, rather than continuously varied, through the flowcell. It is assumed that the minimum of 40 points across a profile accurately represents the continuous changes present under experimental conditions.

Finally, the basis of this model is that concentration gradients formed upon injection are the sole source of refractive index gradients within the flowcell. This cannot be entirely true due to the change in heat upon mixing of these polar solvents coupled with the temperature dependence of refractive index. The possible influence of temperature was investigated by injection of solvents at different temperatures. No visible change in the image size or intensity was observed with temperature fluctuation, and thus the predominant factor influencing the refractive index gradient in these studies was assumed to be the concentration gradient. However, with the knowledge of the refractive index dependence on temperature[20], this model could be modified to investigate this source of detector variability.

CONCLUSIONS

The refractive index response predicted by the dynamic-lens model shows excellent agreement in shape, magnitude, and direction with experimental measurement. This model provides a clearer understanding of the origins of this artifact, which will enable the development of improved flowcell designs for LC. For example, predicted changes in the image size emphasize the practical importance of photodetector size and alignment. In addition, the uniformity of response across the photodiode surface becomes essential when the detected image size and intensity are changing. This model makes possible the evaluation of such practical considerations as source alignment, illumination and collection optics, non-parallel windows and alternate flowcell designs. Equally important is the detailed understanding provided by this model of the factors influencing the refractive index signal. When these artifacts are used for chromatographic measurements, careful interpretation of the signal profile is required. If the peak maximum is used as a measure of retention time, for example, the characterization of column void volume or chromatographic system peaks will be substantially in error. This model is not limited to the simple injection profiles described herein, but is also applicable to more complex profiles arising from stepwise or linear gradient elution[21].

ACKNOWLEDGEMENTS

The authors are grateful to Julie Johnson (Michigan State University) for

technical assistance in implementation of the simulation model, to Jon Wahl (MSU) for the use of the chromatogram in Fig. 1, and to Hugh Montgomery (The Anspec Co.) for the kind loan of the solvent delivery system.

REFERENCES

1 L. R. Snyder and J. J. Kirkland, *Introduction to Modern Liquid Chromatography*, Wiley, New York, NY, 1979, p. 133.
2 D. Betteridge, E. L. Dagless, B. Fields and N. F. Graves, *Analyst (London)*, 103 (1978) 897.
3 D. J. Bornhop and N. J. Dovichi, *Anal. Chem.*, 58 (1986) 504.
4 J. Pawliszyn, *Anal. Chem.*, 58 (1986) 243.
5 J. W. Lyons and L. R. Faulkner, *Anal. Chem.*, 54 (1982) 1960.
6 J. Pawliszyn, *Anal. Chem.*, 58 (1986) 3207.
7 R. Synovec, *Anal. Chem.*, 59 (1987) 2877.
8 Y. F. Cheng and N. J. Dovichi, *Mikrochim. Acta*, 1986III (1986) 351.
9 J. N. Little and G. J. Fallick, *J. Chromatogr.*, 112 (1975) 389.
10 J. E. Stewart, *Appl. Opt.*, 20 (1981) 654.
11 J. E. Stewart, *Anal. Chem.*, 53 (1981) 1125.
12 W. Heller, *J. Phys. Chem.*, 69 (1965) 1123.
13 G. Taylor, *Proc. Roy. Soc. (London)*, A219 (1953) 186.
14 M. J. E. Golay, in D. H. Desty (Editor), *Gas Chromatography 1958*, Academic Press, New York, NY, 1958, p. 36.
15 J. J. VanDeemter, F. J. Zuiderweg and A. Klinkenberg, *Chem. Eng. Sci.*, 5 (1956) 271.
16 J. H. Knox, *J. Chromatogr. Sci.*, 15 (1977) 352.
17 C. R. Wilke and P. Chang, *AIChE J.*, 1 (1955) 264.
18 R. Aris, *Proc. Roy. Soc. (London)*, A235 (1956) 67.
19 K. Peck and M. D. Morris, *J. Chromatogr.*, 448 (1988) 193.
20 N. J. Dovichi, T. G. Nolan and W. A. Weimer, *Anal. Chem.*, 56 (1984) 1700.
21 C. E. Evans and V. L. McGuffin, in preparation.